Pressure tuning of the rare-earth monopnictide DySb

C. Jiang,[1,2] D. Wang,[2] D. S. Wu,[3,4] M. Y. Li,[2] J. L. Luo,[3,4] T. Hu,[5] M. L. Li,[2] W. L. Pei,[1,*] Y. Ding,[2] P. G. Li,[6] Xiao-Jia Chen,[7] and H. Xiao[2,†]

[1]*Key Laboratory of Anisotropy and Texture of Materials (Ministry of Education), Northeastern University, Shenyang 110004, China*
[2]*Center for High Pressure Science and Technology Advanced Research, Beijing 100094, China*
[3]*Beijing National Laboratory for Condensed Matter Physics, Institute of Physics, Chinese Academy of Sciences, P. O. Box 603, Beijing 100190, China*
[4]*School of Physical Sciences, University of Chinese Academy of Sciences, Beijing 100049, China*
[5]*Beijing Academy of Quantum Information Science, Beijing 100193, China*
[6]*Beijing University of Posts and Telecommunications, Beijing 100876, China*
[7]*Department of Physics and Texas Center for Superconductivity, University of Houston, Houston, Texas 77204, USA*

(Received 9 February 2022; revised 3 April 2023; accepted 7 June 2023; published 26 June 2023)

We have systematically investigated the electrical and structural properties of DySb, a potential magnetic topological semimetal, under applied pressure up to 26.8 GPa. At ambient conditions, DySb shows an antiferromagnetic phase transition at $T_N = 10.5$ K. With increasing pressure, T_N shows a nonmonotonic dependence of pressure and arrives the maximum at about 13 GPa. Just above that pressure, we see strong indications of superconductivity (SC) with an onset superconducting transition temperature T_c^{onset} of 2.2 K, concomitant with a structural phase transition from NaCl to CsCl structure. Extreme magnetoresistance as large as $1.4 \times 10^5\%$ is observed at $T = 2$ K and $H = 9$ T at ambient conditions with no sign of saturation. With increasing pressure, magnetoresistance (MR) is greatly suppressed at $P = 13.5$ GPa, around which superconductivity emerges. Thus, DySb provides a good platform to study the relationship among MR, SC, and the structural phase transition.

DOI: 10.1103/PhysRevB.107.214517

I. INTRODUCTION

Rare-earth monopnictide LnPn (for example, Ln = La, Y, Nd, Ce and Pn = P, As, Sb, Bi) compounds have attracted much attention due to their diverse physical properties with simple rock-salt structure [1–9]. A rich magnetic phase diagram is observed in this family owing to the combination of strongly localized f electrons and low-density, high-mobility carriers from the p and d bands [10–13]. The topological semimetal state are observed in LnPn with different magnetic ground states [5,14–17]. The intrinsic topological characteristics are observed in nonmagnetic LaBi [5,14,15]. Angle-resolved photoemission spectroscopy (ARPES) measurements and first principles calculations show the presence of obvious band crossing along the Γ-X direction and an odd number of band inversions [5,14,15]. A topological semimetal state has been observed in NdSb [16] and CeBi [17], which possesses an antiferromagnetic ground state. The extremely large magnetoresistance (XMR) is another important feature of LnPn, which has potential technological applications in electronic devices [10,13,18–22]. An extremely large magnetoresistance of the order of $10^5\%$–$10^6\%$ at 2 K and 9 T is reported in nonmagnetic LaSb and LaBi [21,22]. In CeSb, magnetoresistance (MR) in excess of 1.6×10^6 at fields of 9 T is observed and follows a nonsaturating power law to fields above 30 T [10].

LnPn has pressure-tunable electronic and structural properties. The majority of LnPn compounds undergo the first-order structural phase transition from a NaCl-type (B1) to a CsCl-type (B2) structure at high pressure [2,23]. The pressure suppresses MR significantly, and superconductivity (SC) may be induced. In LaSb, the SC appears at 10.8 GPa, accompanied by a structural phase transition. Thus, the origin of the SC could be related to an enhanced density of states near the Fermi level induced by volume collapse [24]. In YBi, pressure induces the SC at 2.5 GPa and XMR and SC coexist in the phase diagram [25]. The substantially suppressed MR followed by the appearance of SC is observed at about 3.5 GPa in LaBi [4]. In LuBi, the SC emerges at 1.8 GPa and pressure induces two dome-shaped superconducting phases [9], similarly to LaBi, with two superconducting states separated by a first-order structural phase transition [4].

DySb exhibits an antiferromagnetic phase transition at T_N about 10 K and multiple magnetic phase transitions under the magnetic field [1,8,11,26,27]. In most rare-earth monopnictides, the bands with strong spin-orbit coupling show an inversion near the high-symmetry X points, which could host topological phases of correlated electrons [10]. Thus, DySb is a candidate for a magnetic topological semimetal. In this work, we performed systematic high-pressure transport and x-ray diffraction measurements on DySb single-crystal samples. With increasing pressure, T_N shows nonmonotonic dependence on pressure, forming a dome shape. Strong indications

*peiwl@atm.neu.edu.cn
†hong.xiao@hpstar.ac.cn

of superconductivity are found around 14.2 GPa, accompanied by a structural phase transition from a NaCl to a CsCl structure and destruction of XMR. Our results show that MR, SC, and structure are closely related in DySb.

II. EXPERIMENTAL DETAILS

High-quality single crystals of DySb were synthesized using a self-flux method, similarly to synthesizing LaSb [14,28]. Electrical resistivity was measured using a Quantum Design Physical Property Measurement System (PPMS). A dilution refrigerator was used to reach a temperature down to 70 mK. Pressure was applied at room temperature using diamond anvil cells (DAC) made of CuBe alloy, with a 400-μm diameter culet. The DySb sample loaded to the DAC has a thickness of 10 μm. Silicon oil was used as the pressure transmitting medium. Pressure was calibrated using the ruby fluorescence shift at room temperature. We used the van der Pauw method [29] to measure the resistance under pressure. We also performed single-crystal and powder x-ray diffraction measurements on DySb using a symmetric DAC. The data were collected at 296 K on a D8 VENTURE single crystal diffractometer with Mo $K\alpha$ radiation ($\lambda = 0.71073$ Å). Data reduction and empirical absorption correction were performed using the APEX3 program. The structure was solved via an intrinsic phasing method and refined based on the full matrix least-square on F^2 using the SHELXL program.

III. RESULTS AND DISCUSSION

First, the resistance R vs temperature T curve was measured for DySb at ambient conditions as shown in Fig. 1(a). At zero magnetic field, the resistivity decreases monotonically on cooling and shows a sudden drop at T_N about 10.5 K, which is due to the antiferromagnetic phase transition [1,7,8,11]. The residual resistance at 2 K is as small as 5.6×10^{-5} Ω. The residual resistivity ratio RRR is 164, which suggests it is a high-quality sample. By using a dilution refrigerator, we are able to measure the sample down to 70 mK and found that the resistance remains constant in the low-temperature region [Fig. 1(a) and its inset]. The resistance of the plateau in DySb is greatly enhanced in response to a magnetic field. A large magnetoresistance, $\mathrm{MR}(\%) = 100\times\{[R(H) - R(0)]\}/R(0)$ is estimated to be 1.3×10^5 at $T = 2$ K and $H = 9$ T.

A low-temperature resistance plateau is often seen in topological semimetals whose origin is not yet settled. In SmB_6, the resistance plateau is born out of the insulating state at high temperature and attributed to the surface conducting state or possibly the topological surface state [30–32]. In our DySb data, a resistance plateau ($H = 0$) at low temperature is observed emerging from a metallic state, similarly to LaSb [21]. The resistance plateau cannot be explained by the topological surface state, since the bulk state is supposed to dominate the transport properties. Instead, the resistance plateau and XMR could be explained by charge compensation [12,13].

Figure 1(b) shows the resistance measured with an increasing and decreasing magnetic field H at temperatures of $T =$ 2, 4, 9, 20, 50, and 100 K. At low temperatures, $T = 2$ and 4 K, small loops show up in the resistance curve. We made careful measurements with small steps and the loop can be clearly seen in the data. These loops are due to the first-order magnetic phase transition, as shown in the previous report [7,11]. Note that when a magnetic field is applied, DySb undergoes a continuous phase transition to an intermediate phase of the HoP type and then to a fully polarized (ferromagnetic) phase [11]. At high temperatures, there is no hysteresis present in the resistance curves and R shows H^n dependence with the value of n close to 2.

The magnetic field H-dependent Hall resistance R_{xy} was measured at different temperatures, $T = 2$, 3, 4, 5, 6, 7, 8, 9, and 15 K, as shown in Fig. 1(c). For $T < 10$ K, the R_{xy} shows a nonmonotonic H-dependent behavior and changes its sign in the high magnetic field, indicating that the multiple charge carriers presents in the system. In order to clarify the influence of magnetism on the Hall coefficient, we differentiated $R_{xy}(H)$ with respect to the magnetic field H. Figure 1(d) shows the dR_{xy}/dH vs H. At low temperature, the dR_{xy}/dH varies significantly with H, exhibiting large peaks and dips, which diminish with increasing temperature and finally disappear at 15 K. The peaks and dips of dR_{xy}/dH can be interpreted in terms of the magnetic phase transition for the following reason: In general, the Hall resistance has two contributions, one from the normal Hall resistance which is induced by the Lorentz force, and the other one comes from the anomalous Hall resistance, which is proportional to the magnetization, i.e., $R_{xy} = R_{\mathrm{NH}} + R_{\mathrm{AH}}$. The magnetic phase transition induces jumps in magnetization, which causes pronounced changes in R_{AH}. Thus the peaks and dips of dR_{xy}/dH represent the boundary of the magnetic phase. We summarize the peaks (circles) and dips (squares) of dR_{xy}/dH in the H-T phase diagram in the inset to Fig. 1(c). The peaks and dips shown are indeed the phase boundaries of the antiferromagnetic and ferromagnetic phase, respectively, consistent with a recent report [11].

It is worth noting that the magnetic DySb shows XMR similar to the one observed in nonmagnetic LaSb at low temperature, while in DySb the presence of XMR is closely related to the antiferromagnetic transition temperature T_N. The correlation of XMR with the onset of magnetic ordering was previously reported in magnetic CeSb [11]. It was claimed that the XMR of the magnetic and nonmagnetic rare-earth monopnictide systems originate from the semimetallic band structures, but magnetic order can suppress magnetic scattering [11]. Thus, it is expected there is a correlation between XMR and magnetism in DySb. Such a correlation is confirmed by our MR and Hall coefficient data. Figure 1(b) shows that there is a kink in MR, which matches the ferromagnetic phase transition [corresponding to the dip of the Hall coefficient in Fig. 1(d)].

Next, we applied pressure up to 26.8 GPa to DySb single-crystal samples. Figure 2(a) shows the temperature-dependent resistance R curves under different pressures. The antiferromagnetic phase transition temperature T_N shifts to higher temperature and then gets suppressed with further increasing pressure. At $P = 14.2$ GPa, a sharp drop in resistance below the antiferromagnetic phase transition is observed, which is possibly due to pressure induced superconductivity in the system. The arrow indicates the onset superconducting transition temperature T_c^{onset}, which is defined by the temperature at

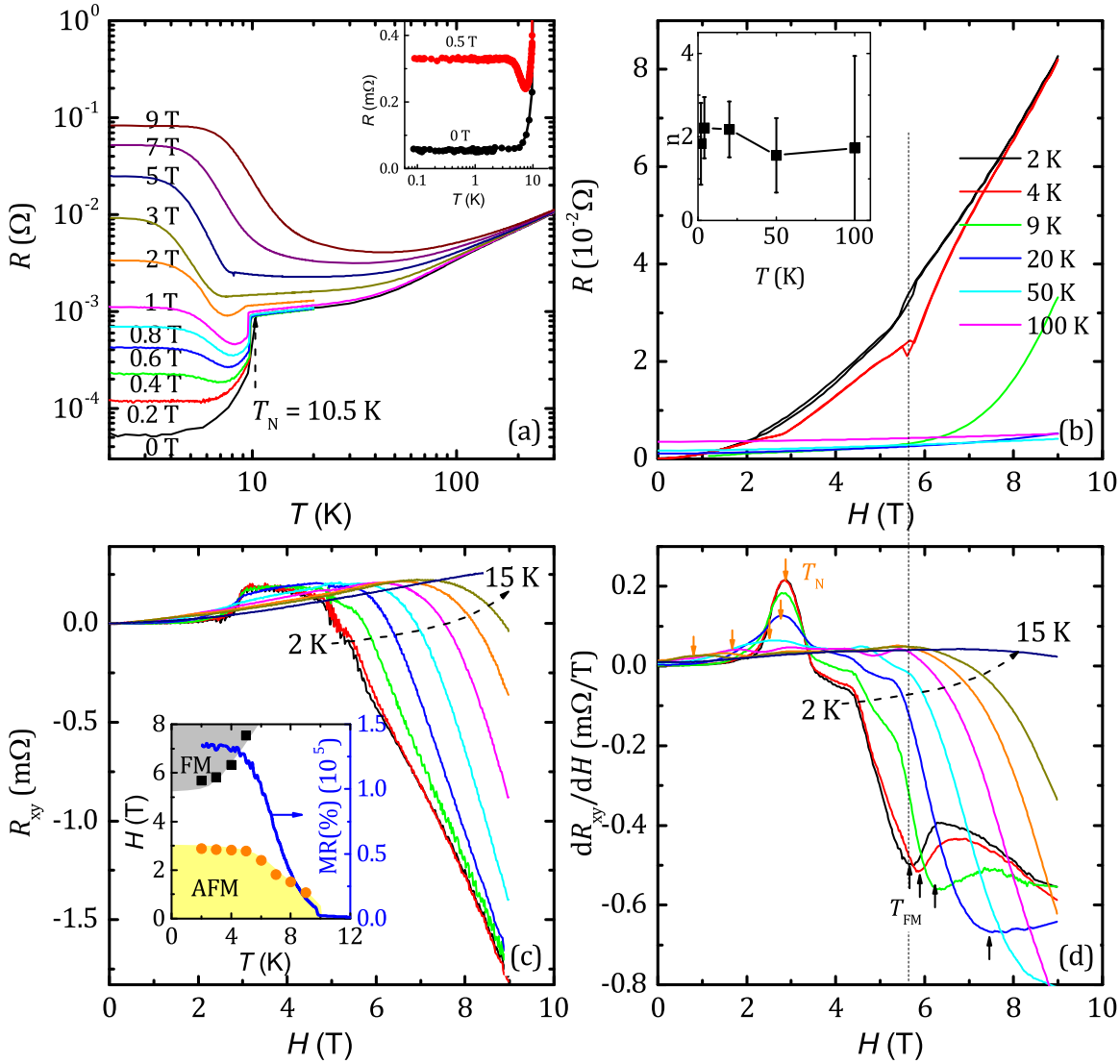

FIG. 1. (a) The temperature T dependence of the resistance R at ambient conditions under different applied magnetic fields $H = 0$, 0.2, 0.4, 0.6, 0.8, 1, 2, 3, 5, 7, and 9 T. The dashed line marks the antiferromagnetic phase transition temperature T_N. The inset shows the enlarged R vs T curves for $H = 0$, and 0.5 T in the low-temperature region. The lowest investigated temperature is down to 70 mK. (b) The resistance R measured with both an increasing and decreasing magnetic field H at different temperatures, $T = 2$, 4, 9, 20, 50, and 100 K. Inset shows the power n (in $R = H^n$) vs T. (c) The Hall resistance R_{xy} vs magnetic field H at different temperatures, $T = 2$, 3, 4, 5, 6, 7, 8, 9, and 15 K. Inset: (left axis) H-T phase diagram of the antiferromagnetism and ferromagnetism; (right axis) temperature dependence of the magnetoresistance. (d) The magnetic field dependence of the derivative of R_{xy} with respect to H. The down arrows marks the antiferromagnetic phase transition temperature T_N and the up arrows signals the ferromagnetic phase transition temperature T_{FM}.

which the resistivity starts to drop. Pressure-induced superconductivity was previously observed in similar compounds, such as LaSb [24], LaBi [4], YBi [25], LuBi [9], and other topological nontrivial material. For example, pressure-driven topological superconductivity is realized in topological insulator Bi_2Te_3 [33], and nearly isotropic superconductivity is found in the layered Weyl semimetal WTe_2 at 9.85 GPa [34].

Figure 2(b) shows the temperature dependence of MR at different pressures. It can be seen that the large MR is present in the temperature region of the resistance plateau, while MR is small in the conventional metallic region. In addition, the upturn at $T < 10$ K in MR is significantly suppressed by pressure. This can be seen more clearly from inset to Fig. 2(b), which shows the pressure dependence of MR at $T = 2$ K. At $P = 13.5$ GPa, the MR is at least three orders of magnitude less than that at ambient conditions. In YBi, the MR shrinks by a factor of two from ambient pressure to $P = 2.6$ GPa, at which superconductivity emerges [25].

Figure 2(c) is the plot of the superconducting transition region for $P = 26.8$ GPa. The magnetic field H suppresses superconductivity and the resistance drop shifts to lower temperature with increasing H. We define the T_c as the temperature at which the resistivity drops to 90% of the normal state resistance, as indicated by the arrow. The upper critical field $H_{c2}(T)$ is plotted in Fig. 2(d) for different applied pressures. For $P = 26.8$ GPa, the T_c is 2.63 K. The $H_{c2}(T)$ data can be described within the entire temperature range by the empirical equation $H_{c2}(T) = H_{c2}(0)(1 - T/T_c)^n$ [inset to

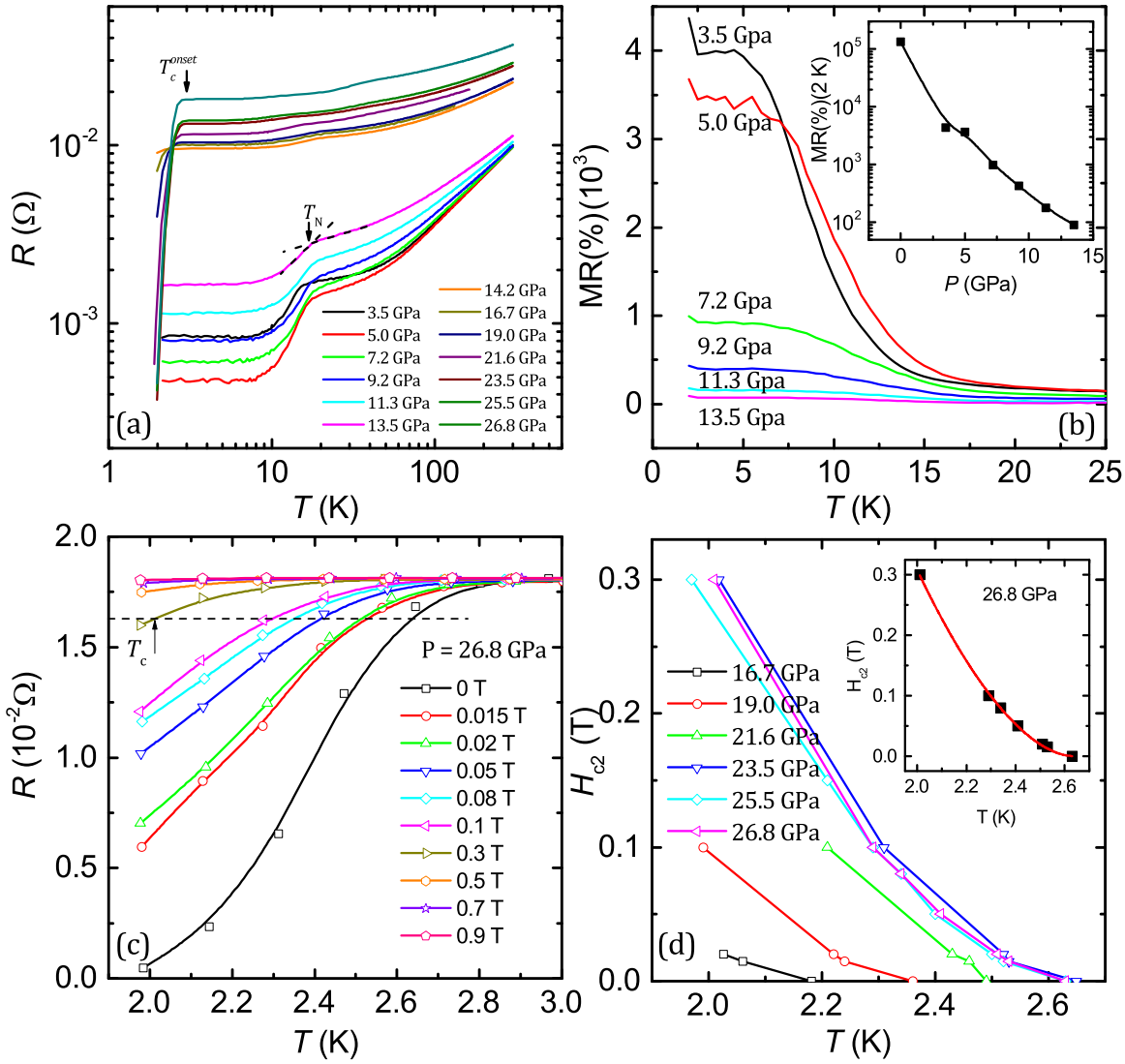

FIG. 2. (a) Temperature (T) dependence of resistance (R) at different pressures, $P = 3.5$, 5.0, 7.2, 9.2, 11.3, 13.5, 14.2, 16.7, 19.0, 21.6, 23.5, 25.5, and 26.8 GPa. The arrows indicate the antiferromagentic phase transition temperature T_N and the onset superconducting transition temperature T_c^{onset}. (b) The T dependence of the magnetoresistance MR. Inset: MR vs P. (c) The plot of the superconducting transition region for $P = 26.8$ GPa under different applied magnetic fields. The arrow denotes the superconducting transition temperature T_c defined as the temperature at which the resistance drops to 90% of the normal state resistance. (d) The temperature dependence of the upper critical field H_{c2} at different pressures, $P = 16.7$, 19.0, 21.6, 23.5, 25.5, and 26.8 GPa.

Fig. 2(d)] [35–37], which gives a H_{c2} of 3.8 T (with the exponent $n = 1.8$), which is below the Pauli paramagnetic limit of a Bardeen-Cooper-Schrieffer weak-coupling superconductor [38]. The value of H_{c2} is larger than that of LaSb [24], for which $H_{c2}(0)$ is estimated to be 0.25 T at 13.7 GPa, but smaller than LuBi [25], for which $H_{c2}(0)$ is 10.4 and 17.3 T at $P = 3$ and 11.5 GPa, respectively. In addition, the H_{c2} is larger for higher T_c. The H_{c2} vs T curves show a clear upward curvature with a high-temperature tail, suggesting a multiband picture in the system [39,40].

Since the experiments cannot be performed below 2 K for the DAC in PPMS, the real zero resistance state is not reached. However, the fact that the temperature at which the resistance starts to drop shifts to a lower temperature with the applied magnetic field, is a good indication of superconducting behavior because the magnetic field will suppress superconductivity. Actually, a pressure-induced superconducting transition accompanied by a structure transition and suppression of XMR has been observed in many topological materials, for example, WTe_2 [41], $ZrTe_5$ [42], $HfTe_5$ [43], LaBi [4], and $NbAs_2$ [44]. Thus, the resistance drop in DySb is most likely due to a superconducting state.

As the the T_c of our sample is relatively close to the expected T_c from antimony, there exists the possibility that the superconductivity emerges from Sb. In Fig. 3, we compare the pressure dependence of the superconducting transition temperature T_c of Sb (data taken from Refs. [45,46]) and DySb (present work). First, the pressure at which superconductivity emerges in Sb and DySb is quite different. In the Sb element, superconductivity appears suddenly at 3.4 K under 5 GPa [46]; while for DySb, superconductivity shows up at 14.2 GPa with a T_c of 2.2 K. Second, multiple phases (phases I, II, III,

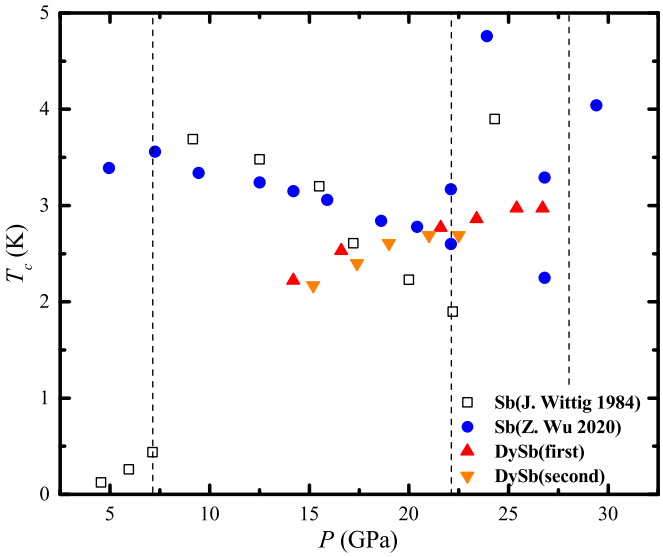

FIG. 3. The pressure P-dependent superconducting transition temperature T_c for Sb (open squares are taken from Ref. [45]; solid circles are taken from Ref. [46]) (we only take data up to 30 GPa since the applied pressure in our measurements is up to 26.8 GPa) and DySb from this work (up and down triangles represent data from first run and second run of experiments).

and IV) are observed in antimony [47], and the series of phase transitions are consistent with the variation of the normal state resistivity at 5 K [46]. In contrast, only two phases are found in DySb, and the pressure of the structural phase transition is consistent with the pressure at which the resistance shows a significant change (between 13.5 and 14.2 GPa). Thus, we can eliminate the effect of Sb on the observed superconductivity.

Note that the electrical resistance behavior changes significantly between 13.5 and 14.2 GPa, where the residual resistance increases discontinuously, the antiferromagnetic drop becomes weaker, and superconductivity appears [Fig. 2(a)]. However at 22 GPa, where previously a structural phase transition is reported to occur [2], no significant anomaly exists in the electrical resistivity and the pressure dependence of T_N and T_c is smooth. On the contrary, in LaSb, the physical properties change, namely by a drop in the residual resistance and magnetoresistance and the appearance of superconductivity, at the structural phase transition pressure. Since the structural phase transition makes the electronic band structure different, it is natural that these properties change with the structural phase transition. However, in this study, the T_N and T_c do not change much at 22 GPa. These facts raise the suspicion that the structural phase transition in our sample may occur between 13.5 and 14.2 GPa.

To clarify the causes for the significant change in the behavior of the electrical resistance between 13.5 and 14.2 GPa, we performed x-ray diffraction measurements on DySb both at ambient conditions and under high pressure up to 23.3 GPa. At ambient pressure, we performed x-ray diffraction measurements on a single-crystal sample of DySb. Figure 4 shows the optical photo of DySb single crystal sample used in the experiment, the processed diffraction spots, and the crystal structure of DySb. DySb crystallizes in the space group Fm-3m of cubic

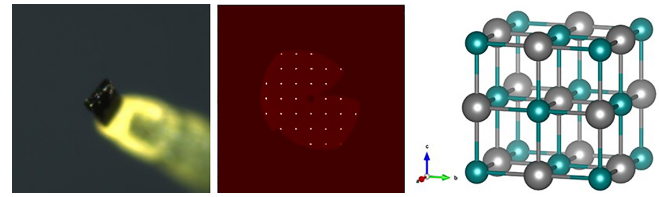

FIG. 4. (a) Optical photo of the DySb single crystal used in the single crystal diffraction experiment. (b) Processed diffraction spots of (hk0) crystal plane, and the best resolution is 0.49 angstrom. (c) Crystal structure of DySb determined by single crystal refinement; the picture is drawn by VESTA software, and the light blue and gray spheres represent the Dy and Sb atoms, respectively.

system. There is one independent Dy site (4*a Wyckoff* position) and one independent Sb site (4*b Wyckoff* position). The detailed structural parameters at ambient pressures are listed in Table I. In order to verify the structural transformation induced by pressure, a single crystal with a regular shape was selected and ground into powder, and the same diffractometer was used for powder x-ray diffraction measurements. Figure 5 shows the powder x-ray diffraction pattern of DySb. It can be seen that with increasing pressure, the diffraction peak of the (200) crystal plane in the NaCl-type structure shifts to high angle until a new diffraction peak begins to appear at 14.8 GPa, i.e., a structural transformation begins. The intensity of the new diffraction peak gradually increases with increasing pressure. For $P >$ 14.8 GPa, the sample enters the two-phase coexistence region. We also carried out single-crystal diffraction experiments to analyze the structural phase composition under pressure. Figures 5(b) and 5(c) shows selected data at two different pressures, 7.5 and 11.3 GPa. The experimental data were well matched with the refined cubic structure model (space group Fm-3m) using Rietveld refinement performed on Fullprof software. The R factors after refinement under two pressure are $R_p = 1.89\%$, $R_{wp} = 3.24\%$ ($P = 7.5$ GPa), and $R_p = 1.38\%$, $R_{wp} = 2.25\%$ ($P = 11.3$ GPa).

Our result of a structural phase transition at 14.8 GPa seems to be different from the previous report [2] where the structural phase transition is reported to occur at about 22 GPa. We compare the pressure dependence of the lattice constant in our work and Ref. [2] (see Fig. S1 of the Supplemental Materials [48]). It is found that although the claimed pressure is different, the structural phase transition occurs at the same value of lattice constant in both cases. This indicates that the effective pressure is the same for the structural phase transition in our work and the reference [2]. Note that high-pressure measurements are very challenging, and there are many reasons why the measured pressure might

TABLE I. Structural parameters of DySb determined by single crystal XRD measurements at 296 K. Space group: Fm-3m. Lattice parameter: $a = 6.1639(19)$ Å.

Atom	Wyckoff site.	x	y	z	U^*_{iso}/U_{eq}
Dy	4a	1/2	1/2	1/2	0.0121(11)
Sb	4b	1/2	1	1/2	0.0118(10)

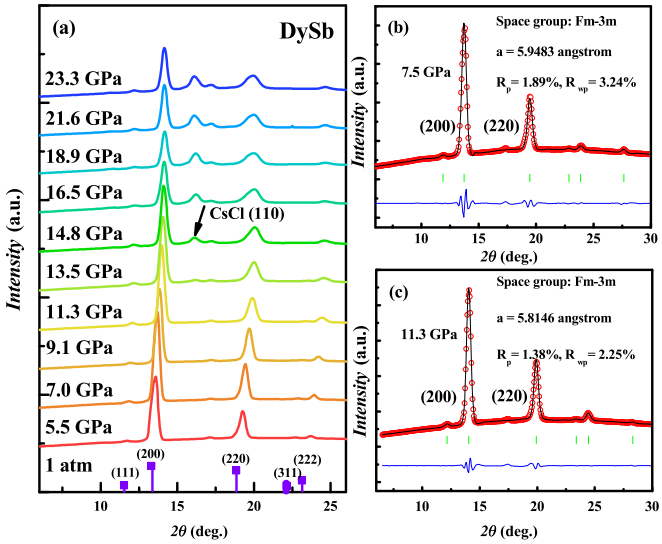

FIG. 5. (a) XRD pattern of DySb powder under high pressure. [(b) and (c)] Refined XRD patterns of DySb single crystal at $P =$ 7.5 GPa and 11.3 GPa, respectively.

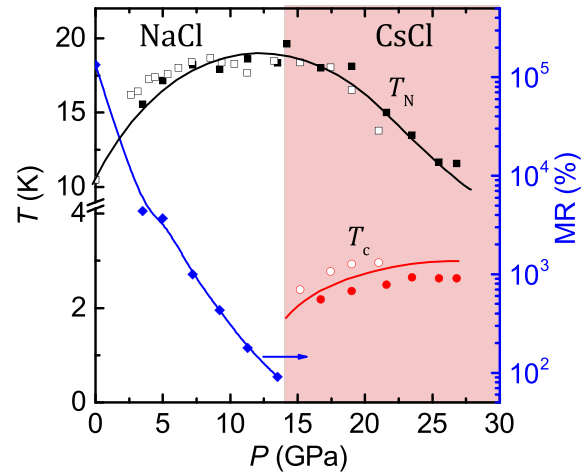

FIG. 6. The temperature T vs pressure P phase diagram and the pressure-dependent meganetoresistance MR of DySb. The open and solid symbols represent data from two different runs. The squares represent the antiferromagnetic phase transition temperature T_N. The circles denotes the superconducting transition temperature T_c. The diamonds are the magnetoresistance MR. Above ∼14 GPa, the high-pressure CsCl structure emerges.

be off. The difference in the value of the "nominal" pressure could be due to technical details in pressurizing the sample, the various types of pressure cell, transmitting medium, pressure calibration method, and inhomogeneity of the pressure distribution inside the sample chamber of the cell under high pressure. We listed the structural phase transition pressure for similar compounds from different reports (see Table S2 of the Supplemental Material [48] and Refs. [2,49–52]). The difference in pressures reported is as large as 7 GPa.

Figure 6 shows the pressure dependence of the antiferromagnetic phase transition temperature T_N (left axis), the superconducting transition temperature T_c (left axis), and magnetoresistance MR (right axis). T_N first increases with increasing pressure and then decreases with further increasing pressure, forming a dome shape. The MR was quickly suppressed with pressure. From ambient conditions to $P =$ 13.5 GPa, MR (at $T = 2$ K and $H = 9$ T) changes from 1.4×10^5% to 90%. Accompanying the significant suppression of the MR, superconductivity emerges at $P = 14.2$ GPa. A structural phase transition from low-pressure NaCl to high-pressure CsCl structure is observed around the same pressure. Note that the superconductivity emerges in the high-pressure phase. In DySb, the structural phase transition is observed at a consistent pressure with the pressure for the significant resistance change and the appearance of superconductivity, similarly to LaSb [24].

Theoretically, a band reversion is found in DySb, which suggests that DySb might be a magnetic Weyl semimetal. However, the inversion is seated about 0.34 eV below the Fermi level [7], which is difficult to be detected by transport measurements and seems to exclude the topological nature of XMR. The band topological properties are usually determined according to the ARPES measurements or Shubnikov de-Haas (SdH) oscillations in the magnetoresistance. In this work, our magnetic field is limited to 9 T and the magnetoresistance does not show SdH oscillation. Thus, it is hard to judge whether DySb is of trivial or nontrivial topological structure. Further measurements under high magnetic field with analysis of the Berry phase is required to confirm if DySb is topological nontrivial.

IV. CONCLUSIONS

In summary, we investigated the properties of DySb both at ambient conditions and under applied pressure. A resistance plateau persists down to 70 mK and extreme magetoresistance is present in the low-temperature region below 10 K. A structural phase transition from the NaCl to the CsCl structure occurs under pressure (∼14 GPa). Strong indications of superconductivity emerges in the high-pressure phase. The magnetoresistance was substantially suppressed, at the same pressure where the structural phase transition starts and the superconductivity emerges. Based on our data, we constructed a temperature-pressure phase diagram of the magnetic and superconducting phases. Our results show the intimate relationship between superconductivity, magnetoresistance and the structural phase transition. As a potential magnetic topological semimetal, DySb deserves further study, which may lead to topologically driven spintronics.

ACKNOWLEDGMENTS

Work at HPSTAR was supported by NSAF Grant No. U1530402. Work at BAQIS was supported by NSFC Grant No. 11574338. W. L. Pei acknowledges the support from NSFC Grant No. 52071070.

[1] E. Bucher, R. J. Birgeneau, J. P. Maita, G. P. Felcher, and T. O. Brun, Magnetic and Structural Phase Transition in DySb, Phys. Rev. Lett. **28**, 746 (1972).

[2] I. Shirotani, J. Hayashi, K. Yamanashi, N. Ishimatsu, O. Shimomura, and T. Kikegawa, Pressure-induced phase transitions in lanthanide monoantimonides with a NaCl-type structure, Phys. Rev. B **64**, 132101 (2001).

[3] Y. Wu, Y. Lee, T. Kong, D. Mou, R. Jiang, L. Huang, S. L. Bud'ko, P. C. Canfield, and A. Kaminski, Electronic structure of rSb (r = Y, Ce, Gd, Dy, Ho, Tm, Lu) studied by angle-resolved photoemission spectroscopy, Phys. Rev. B **96**, 035134 (2017).

[4] F. F. Tafti, M. S. Torikachvili, R. L. Stillwell, B. Baer, E. Stavrou, S. T. Weir, Y. K. Vohra, H.-Y. Yang, E. F. McDonnell, S. K. Kushwaha, Q. D. Gibson, R. J. Cava, and J. R. Jeffries, Tuning the electronic and the crystalline structure of labi by pressure: From extreme magnetoresistance to superconductivity, Phys. Rev. B **95**, 014507 (2017).

[5] R. Lou, B.-B. Fu, Q. N. Xu, P.-J. Guo, L.-Y. Kong, L.-K. Zeng, J.-Z. Ma, P. Richard, C. Fang, Y.-B. Huang, S.-S. Sun, Q. Wang, L. Wang, Y.-G. Shi, H. C. Lei, K. Liu, H. M. Weng, T. Qian, H. Ding, and S.-C. Wang, Evidence of topological insulator state in the semimetal LaBi, Phys. Rev. B **95**, 115140 (2017).

[6] X. Duan, F. Wu, J. Chen, P. Zhang, Y. Liu, H. Yuan, and C. Cao, Tunable electronic structure and topological properties of LnPn (Ln=Ce, Pr, Sm, Gd, Yb; Pn=Sb, Bi), Commun. Phys. **1**, 71 (2018).

[7] D. D. Liang, Y. J. Wang, C. Y. Xi, W. L. Zhen, J. Yang, L. Pi, W. K. Zhu, and C. J. Zhang, Extreme magnetoresistance and Shubnikov-de Haas oscillations in ferromagnetic DySb, APL Mater. **6**, 086105 (2018).

[8] W. J. Ban, D. S. Wu, B. Xu, J. L. Luo, and H. Xiao, Revealing 'plasmaron' feature in DySb by optical spectroscopy study, J. Phys.: Condens. Matter **31**, 405701 (2019).

[9] H. Gu, F. Tang, Y.-R. Ruan, J.-M. Zhang, R.-J. Tang, W. Zhao, R. Zhao, L. Zhang, Z.-D. Han, B. Qian, X.-F. Jiang, and Y. Fang, Pressure effect on the topologically nontrivial electronic state and transport of lutecium monobismuthide, Phys. Rev. Mater. **4**, 124204 (2020).

[10] L. Ye, T. Suzuki, C. R. Wicker, and J. G. Checkelsky, Extreme magnetoresistance in magnetic rare-earth monopnictides, Phys. Rev. B **97**, 081108(R) (2018).

[11] W. Liu, D. Liang, F. Meng, J. Zhao, W. Zhu, J. Fan, L. Pi, C. Zhang, L. Zhang, and Y. Zhang, Field-induced tricritical phenomenon and multiple phases in DySb, Phys. Rev. B **102**, 174417 (2020).

[12] P.-J. Guo, H.-C. Yang, B.-J. Zhang, K. Liu, and Z.-Y. Lu, Charge compensation in extremely large magnetoresistance materials LaSb and LaBi revealed by first-principles calculations, Phys. Rev. B **93**, 235142 (2016).

[13] L.-K. Zeng, R. Lou, D.-S. Wu, Q. N. Xu, P.-J. Guo, L.-Y. Kong, Y.-G. Zhong, J.-Z. Ma, B.-B. Fu, P. Richard, P. Wang, G. T. Liu, L. Lu, Y.-B. Huang, C. Fang, S.-S. Sun, Q. Wang, L. Wang, Y.-G. Shi, H. M. Weng *et al.*, Compensated Semimetal LaSb with Unsaturated Magnetoresistance, Phys. Rev. Lett. **117**, 127204 (2016).

[14] X. H. Niu, D. F. Xu, Y. H. Bai, Q. Song, X. P. Shen, B. P. Xie, Z. Sun, Y. B. Huang, D. C. Peets, and D. L. Feng, Presence of exotic electronic surface states in LaBi and LaSb, Phys. Rev. B **94**, 165163 (2016).

[15] J. Nayak, S.-C. Wu, N. Kumar, C. Shekhar, S. Singh, J. Fink, E. E. D. Rienks, G. H. Fecher, S. S. P. Parkin, B. Yan, and C. Felser, Multiple dirac cones at the surface of the topological metal LaBi, Nat. Commun. **8**, 13942 (2017).

[16] Y. Wang, J. H. Yu, Y. Q. Wang, C. Y. Xi, L. S. Ling, S. L. Zhang, J. R. Wang, Y. M. Xiong, T. Han, H. Han, J. Yang, J. Gong, L. Luo, W. Tong, L. Zhang, Z. Qu, Y. Y. Han, W. K. Zhu, L. Pi, X. G. Wan *et al.*, Topological semimetal state and field-induced Fermi surface reconstruction in the antiferromagnetic monopnictide NdSb, Phys. Rev. B **97**, 115133 (2018).

[17] H. Oinuma, S. Souma, K. Nakayama, K. Horiba, H. Kumigashira, M. Yoshida, A. Ochiai, T. Takahashi, and T. Sato, Unusual change in the dirac-cone energy band upon a two-step magnetic transition in CeBi, Phys. Rev. B **100**, 125122 (2019).

[18] N. Wakeham, E. D. Bauer, M. Neupane, and F. Ronning, Large magnetoresistance in the antiferromagnetic semimetal NdSb, Phys. Rev. B **93**, 205152 (2016).

[19] F. Wu, C. Y. Guo, M. Smidman, J. L. Zhang, and H. Q. Yuan, Large magnetoresistance and Fermi surface topology of PrSb, Phys. Rev. B **96**, 125122 (2017).

[20] C. Guo, C. Cao, M. Smidman, F. Wu, Y. Zhang, F. Steglich, F.-C. Zhang, and H. Yuan, Possible Weyl fermions in the magnetic kondo system CeSb, npj Quant. Mater. **2**, 39 (2017).

[21] F. F. Tafti, Q. D. Gibson, S. K. Kushwaha, N. Haldolaarachchige, and R. J. Cava, Resistivity plateau and extreme magnetoresistance in LaSb, Nat. Phys. **12**, 272 (2016).

[22] F. Fallah Tafti, Q. Gibson, S. Kushwaha, J. W. Krizan, N. Haldolaarachchige, and R. J. Cava, Temperature-field phase diagram of extreme magnetoresistance, Proc. Natl. Acad. Sci. USA **113**, E3475 (2016).

[23] D. C. Gupta and S. Kulshrestha, Dysb under high pressures: A full-potential study, J. Alloys Compd. **509**, 4653 (2011).

[24] M. Zhang, X. Wang, A. Rahman, R. Dai, Z. Wang, and Z. Zhang, Observation of superconductivity accompanying the pressure-induced structural phase transition in LaSb, Phys. Rev. B **101**, 064106 (2020).

[25] C. Q. Xu, B. Li, M. R. van Delft, W. H. Jiao, W. Zhou, B. Qian, N. D. Zhigadlo, D. Qian, R. Sankar, N. E. Hussey, and X. Xu, Extreme magnetoresistance and pressure-induced superconductivity in the topological semimetal candidate YBi, Phys. Rev. B **99**, 024110 (2019).

[26] W. J. Hu, J. Du, B. Li, Q. Zhang, and Z. D. Zhang, Giant magnetocaloric effect in the ising antiferromagnet DySb, Appl. Phys. Lett. **92**, 192505 (2008).

[27] D. Li, S. Nimori, and T. Shikama, Giant and anisotropic magnetocaloric effect in antiferromagnetic single crystalline DySb, Solid State Commun. **150**, 1865 (2010).

[28] P. C. Canfield and Z. Fisk, Growth of single crystals from metallic fluxes, Philos. Mag. B **65**, 1117 (1992).

[29] L. J. van der Pauw, A method of measuring the resistivity and Hall coefficient on lamellae of arbitrary shape, Philips Tech. Rev. **20**, 220 (1958).

[30] D. J. Kim, S. Thomas, T. Grant, J. Botimer, Z. Fisk, and J. Xia, Surface Hall effect and nonlocal transport in SmB_6: Evidence for surface conduction, Sci. Rep. **3**, 3150 (2013).

[31] D. J. Kim, J. Xia, and Z. Fisk, Topological surface state in the Kondo insulator samarium hexaboride, Nat. Mater. **13**, 466 (2014).

[32] S. Wolgast, C. Kurdak, K. Sun, J. W. Allen, D.-J. Kim, and Z. Fisk, Low-temperature surface conduction in the Kondo insulator SmB_6, Phys. Rev. B **88**, 180405(R) (2013).

[33] J. L. Zhang, S. J. Zhang, H. M. Weng, W. Zhang, L. X. Yang, Q. Q. Liu, S. M. Feng, X. C. Wang, R. C. Yu, L. Z. Cao, L. Wang, W. G. Yang, H. Z. Liu, W. Y. Zhao, S. C. Zhang, X. Dai, Z. Fang, and C. Q. Jin, Pressure-induced superconductivity in topological parent compound Bi_2Te_3, Proc. Natl. Acad. Sci. USA **108**, 24 (2011).

[34] Y. T. Chan, P. L. Alireza, K. Y. Yip, Q. Niu, K. T. Lai, and S. K. Goh, Nearly isotropic superconductivity in the layered Weyl semimetal WTe_2 at 98.5 kbar, Phys. Rev. B **96**, 180504(R) (2017).

[35] X.-C. Pan, X. Chen, H. Liu, Y. Feng, Z. Wei, Y. Zhou, Z. Chi, L. Pi, F. Yen, F. Song, X. Wan, Z. Yang, B. Wang, G. Wang, and Y. Zhang, Pressure-driven dome-shaped superconductivity and electronic structural evolution in tungsten ditelluride, Nat. Commun. **6**, 7805 (2015).

[36] B. Gao, Y. Ma, G. Mu, and H. Xiao, Pressure-induced superconductivity in parent CaFeAsF single crystals, Phys. Rev. B **97**, 174505 (2018).

[37] O. Pavlosiuk, D. Kaczorowski, and P. Wiśniewski, Shubnikov–de Haas oscillations, weak antilocalization effect and large linear magnetoresistance in the putative topological superconductor LuPdBi, Sci. Rep. **5**, 9158 (2015).

[38] A. M. Clogston, Upper limit for the critical field in hard superconductors, Phys. Rev. Lett. **9**, 266 (1962).

[39] H. Xiao, T. Hu, A. P. Dioguardi, N. apRoberts-Warren, A. C. Shockley, J. Crocker, D. M. Nisson, Z. Viskadourakis, X. Tee, I. Radulov, C. C. Almasan, N. J. Curro, and C. Panagopoulos, Evidence for filamentary superconductivity nucleated at antiphase domain walls in antiferromagnetic $CaFe_2As_2$, Phys. Rev. B **85**, 024530 (2012).

[40] H. Xiao, T. Hu, S. K. He, B. Shen, W. J. Zhang, B. Xu, K. F. He, J. Han, Y. P. Singh, H. H. Wen, X. G. Qiu, C. Panagopoulos, and C. C. Almasan, Filamentary superconductivity across the phase diagram of $Ba(Fe, Co)_2As_2$, Phys. Rev. B **86**, 064521 (2012).

[41] D. Kang, Y. Zhou, W. Yi, C. Yang, J. Guo, Y. Shi, S. Zhang, Z. Wang, C. Zhang, S. Jiang, A. Li, K. Yang, Q. Wu, G. Zhang, L. Sun, and Z. Zhao, Superconductivity emerging from a suppressed large magnetoresistant state in tungsten ditelluride, Nat. Commun. **6**, 7804 (2015).

[42] Y. Zhou, J. Wu, W. Ning, N. Li, Y. Du, X. Chen, R. Zhang, Z. Chi, X. Wang, X. Zhu, P. Lu, C. Ji, X. Wan, Z. Yang, J. Sun, W. Yang, M. Tian, Y. Zhang, and H.-K. Mao, Pressure-induced superconductivity in a three-dimensional topological material $ZrTe_5$, Proc. Natl. Acad. Sci. USA **113**, 2904 (2016).

[43] Y. Qi, W. Shi, P. G. Naumov, N. Kumar, W. Schnelle, O. Barkalov, C. Shekhar, H. Borrmann, C. Felser, B. Yan, and S. A. Medvedev, Pressure-driven superconductivity in the transition-metal pentatelluride $HfTe_5$, Phys. Rev. B **94**, 054517 (2016).

[44] Y. Li, C. An, C. Hua, X. Chen, Y. Zhou, Y. Zhou, R. Zhang, C. Park, Z. Wang, Y. Lu, Y. Zheng, Z. Yang, and Z.-A. Xu, Pressure-induced superconductivity in topological semimetal NbAs2, npj Quant. Mater. **3**, 58 (2018).

[45] J. Wittig, Superconductivity in elements and binary systems at high pressure, Mater. Res. Soc. Symp. Proc. **22**, 17 (1984).

[46] Z. Wu, L. Deng, M. Gooch, S. Huyan, and C. Chu, The retention at ambient of the high-pressure-induced metastable superconducting phases in antimony single crystals, Mater. Today Phys. **15**, 100291 (2020).

[47] O. Degtyareva, M. I. McMahon, and R. J. Nelmes, Pressure-induced incommensurate-to-incommensurate phase transition in antimony, Phys. Rev. B **70**, 184119 (2004).

[48] See Supplemental Material at http://link.aps.org/supplemental/10.1103/PhysRevB.107.214517 for comparason of the pressure dependence of the lattice constant in our work and in Ref. [2] and also for the structural phase transition pressure for similar compounds fromdifferent reports.

[49] I. Shirotani, J. Hayashi, K. Yamanashi, K. Hirano, T. Adachi, N. Ishimatsu, O. Shimomura, and T. Kikegawa, X-ray study with synchrotron radiation of cerium and praseodymium monopnictides with the NaCl-type structure at high pressures, Phys. B: Condens. Matter **334**, 167 (2003).

[50] I. Vedel, A. M. Redon, J. Rossat-Mignod, O. Vogt, and J.-M. Leger, Electronic and crystallographic transitions induced by pressure in CeP, J. Phys. C **20**, 3439 (1987).

[51] A. Werner, H. Hochheimer, R. Meng, and E. Bucher, Absence of pressure-induced valence change in CeAs, Phys. Lett. A **97**, 207 (1983).

[52] J. Leger, D. Ravot, and J. Rossat-Mignod, Volume behaviour of CeSb and LaSb up to 25 GPa, J. Phys. C **17**, 4935 (1984).